Efficient Maximum-Likelihood Based Clock and Phase Estimators for OQPSK Signals

Antonio A. D'Amico

***Abstract*—In this paper we propose an algorithm for joint carrier phase and timing estimation with OQPSK modulations. The derivation is based on the maximum-likelihood criterion, and exploits a very efficient algorithm for the detection of differentially encoded M-PSK symbols already described in literature. Though we are mainly interested in measuring the phase and clock parameters, estimates of the transmitted symbols are also obtained as by-products. The resulting scheme has a feedforward structure and provides phase and timing information in a fixed time, differently from closed-loop architectures. It can be implemented in digital form and is particularly suitable for burst mode transmissions. Its performance is investigated by simulation and the results are compared with Cramér-Rao bounds. It turns out that the estimation accuracy is very close to the theoretical limits, even with short observation intervals and small values of the excess bandwidth. In such conditions, the proposed estimators largely outperform other schemes already known in literature. Their superiority becomes less significant as the signal bandwidth increases.**

I. Introduction

Offset quadriphase modulation (OQPSK) is similar to conventional QPSK, except that the information stream on the sine carrier is delayed $T/2$ seconds from that on the cosine carrier, with T being the symbol period. As a result, bandlimited OQPSK signals present a maximum envelope variation of only 3 dB (70%), as opposed to 100% with QPSK. This is a very appealing feature, especially in those applications where power-efficient amplifiers must be used. Indeed, with filtered QPSK the amplifier nonlinearity causes a significant regeneration of the signal spectrum due to the envelope variations, whereas fairly limited sidelobe regrowth is observed with OQPSK [1]–[3].

Differently from non-offset modulations, for which various timing estimation algorithms with very good performance are available [4]–[9], a few estimators have been proposed in literature for OQPSK signals [10]–[13]. Essentially, the main difficulties in synchronizing offset signals derive from the clock recovery sensitivity to the carrier phase [10], and indeed the best schemes known in literature for OQPSK are the joint phase and timing estimators proposed in [12], [13]. They both have a feedforward structure, and can be implemented in digital form with a sampling frequency of $2/T$ for the system in [12] and $4/T$ for the other. Though they have good performance (in particular the clock estimator) with signals whose excess bandwidth is greater than 0.5, their accuracy considerably worsens as the rolloff decreases, especially with short observation intervals. Good performance with small excess bandwidths can be obtained, in principle, with closed-loop decision-directed architectures such as those described in [14, Section 8.6]. However, in this case long acquisitions are expected, due to the strong interactions between phase and timing loops, which may not be compatible with short data packets in burst mode transmissions.

In this paper we propose an algorithm for joint phase and timing estimation (and data detection) with OQPSK signals. It is derived by maximizing the likelihood function (LF) with respect to all the unknown parameters contained in the received signal, including the information bits transmitted on the in-phase and quadrature channels. Despite the apparently exponential complexity of the problem, it can be solved efficiently using the algorithm proposed by Mackenthun in [15] for the detection of differentially encoded M-PSK constellations. The resulting scheme can be easily implemented in digital form, and has a feedforward structure in which the timing information is first extracted from asynchronous samples of the received signal, in a phase-less fashion. Data detection and phase estimation are then performed on *synchronized* samples that can be obtained from the same asynchronous samples previously used for clock recovery.

Compared to other algorithms already known in literature (e.g. [10]–[13]), the proposed estimator has remarkably better performance especially with short observation intervals and small excess bandwidths. Hence, it is particularly appealing for burst mode transmissions where rapid acquisitions are required. Though the present schemes are proposed for OQPSK signals, they can be easily extended to M-PSK modulations.

The main result of this work can then be summarized as follows: we show that efficient synchronization (i.e. with estimation performance very close to the Cramér-Rao bounds) of OQPSK signals is possible even with short observation intervals and small excess bandwidths, with an acceptable complexity.

The paper is organized as follows. In the next section we introduce the signal model, and we derive the concentrated likelihood functions (CLFs) for carrier phase estimation, data detection and timing recovery. In Section III an approximate procedure for maximizing the timing CLF is proposed and discussed. The location of the maximum, which is expressed in closed-form as a function of asynchronous signal samples, is used as an estimator for the unknown timing parameter. Simulation results and comparisons with existing algorithms are reported in Section IV. Conclusions are finally drawn in Section V.

The author is with the Department of Information Engineering, Via Caruso 16, 56100 Pisa, Italy. E-mail:antonio.damico@iet.unipi.it

II. Signal Model

An OQPSK signal can be written in complex form as

$$s(t) = \sum_i a_i g(t - iT) + j \sum_i b_i g(t - T/2 - iT) \quad (1)$$

where $g(t)$ is a real-valued signaling pulse with energy E_g, T is the signaling interval, and $\mathbf{a} = \{a_i\}$ and $\mathbf{b} = \{b_i\}$ represent the data symbols on the in-phase and quadrature channels. They are independent, identically distributed and take on the values ± 1 with equal probability. Without loss of generality, we assume $E_g = 1$.

After demodulation, the received waveform $r(t)$ consists of the signal in (1) plus noise $w(t)$. The noise component is modeled as a complex-valued white Gaussian process with independent real and imaginary parts, each with two sided power spectral density N_0. We also assume a flat-fading channel model, and hence the received waveform can formally be written as

$$r(t) = he^{j\theta} s(t - \tau) + w(t) \quad (2)$$

where the *real* parameters $h > 0$, θ, and τ are the attenuation, phase shift, and time delay, respectively, due to the propagation channel. It is assumed that the channel coherence-time is much longer than the observation interval, so that h, θ, and τ can be treated as constants.

Parameters h, θ, τ, $\mathbf{a}$, and $\mathbf{b}$ are all unknown at the receiver, and must be estimated. Actually, in this study we are mainly interested in the estimation of θ and τ, even though estimates of h, $\mathbf{a}$, and $\mathbf{b}$ will be obtained as by-products. This problem is addressed by resorting to the maximum likelihood (ML) criterion. For this purpose, we assume that the received signal $r(t)$ is observed in the interval $[0, T_0)$, where $T_0 = L_0 T$ with $L_0 \in \mathbb{N}$. Then, the ML function for the estimation of the unknown parameters takes the form [16]

$$\begin{aligned}\Lambda(\tilde{\mathbf{a}}, \tilde{\mathbf{b}}, \tilde{h}, \tilde{\theta}, \tilde{\tau}) = 2\tilde{h}\mathrm{Re}\left\{ e^{-j\tilde{\theta}} \int_0^{T_0} r(t)\tilde{s}^*(t - \tilde{\tau})dt \right\} \\ - \tilde{h}^2 \int_0^{T_0} |\tilde{s}(t - \tilde{\tau})|^2 \, dt\end{aligned} \quad (3)$$

where

$$\tilde{s}(t) = \sum_i \tilde{a}_i g(t - iT) + j \sum_i \tilde{b}_i g(t - T/2 - iT), \quad (4)$$

z^* is the conjugate of z, and notations of the type $\tilde{p}$ are used to indicate a possible value of parameter p. The ML estimates of $\mathbf{a}$, $\mathbf{b}$, h, θ and τ, are found by maximimizing $\Lambda(\tilde{\mathbf{a}}, \tilde{\mathbf{b}}, \tilde{h}, \tilde{\theta}, \tilde{\tau})$ with respect to $\tilde{\mathbf{a}}$, $\tilde{\mathbf{b}}$, $\tilde{h}$, $\tilde{\theta}$ and $\tilde{\tau}$, i.e.

$$(\hat{\mathbf{a}}, \hat{\mathbf{b}}, \hat{h}, \hat{\theta}, \hat{\tau}) = \arg \max_{\tilde{\mathbf{a}}, \tilde{\mathbf{b}}, \tilde{h}, \tilde{\theta}, \tilde{\tau}} \Lambda(\tilde{\mathbf{a}}, \tilde{\mathbf{b}}, \tilde{h}, \tilde{\theta}, \tilde{\tau}) \quad (5)$$

To proceed further we fix $\tilde{\mathbf{a}}, \tilde{\mathbf{b}}, \tilde{h}, \tilde{\tau}$ and we search for the maximum of (3) with respect to $\tilde{\theta}$. To this end, we rewrite (3) as follows

$$\begin{aligned}\Lambda(\tilde{\mathbf{a}}, \tilde{\mathbf{b}}, \tilde{h}, \tilde{\theta}, \tilde{\tau}) = 2\tilde{h}\mathrm{Re}\left\{ e^{-j[\tilde{\theta} - \vartheta(\tilde{\mathbf{a}}, \tilde{\mathbf{b}}, \tilde{\tau})]} \left| \int_0^{T_0} r(t)\tilde{s}^*(t - \tilde{\tau})dt \right| \right\} \\ - \tilde{h}^2 \int_0^{T_0} |\tilde{s}(t - \tilde{\tau})|^2 \, dt\end{aligned} \quad (6)$$

where

$$\vartheta(\tilde{\mathbf{a}}, \tilde{\mathbf{b}}, \tilde{\tau}) = \arg\left\{ \int_0^{T_0} r(t)\tilde{s}^*(t - \tilde{\tau})dt \right\} \quad (7)$$

and $\arg\{z\}$ is the argument of the complex number z. The maximization of (6) with respect to $\tilde{\theta}$ is straightforward now. Indeed, since neither $\vartheta(\tilde{\mathbf{a}}, \tilde{\mathbf{b}}, \tilde{\tau})$ nor $\left| \int_0^{T_0} r(t)\tilde{s}^*(t - \tilde{\tau})dt \right|$ depends on $\tilde{\theta}$ then the maximum of (6) is achieved for

$$\tilde{\theta} = \vartheta(\tilde{\mathbf{a}}, \tilde{\mathbf{b}}, \tilde{\tau}) \quad (8)$$

Using (8) in (6) gives the concentrated likelihood function for the estimation of $\mathbf{a}$, $\mathbf{b}$, h and τ, i.e.

$$\Lambda(\tilde{\mathbf{a}}, \tilde{\mathbf{b}}, \tilde{h}, \tilde{\tau}) = 2\tilde{h} \left| \int_0^{T_0} r(t)\tilde{s}^*(t - \tilde{\tau})dt \right| - \tilde{h}^2 \int_0^{T_0} |\tilde{s}(t - \tilde{\tau})|^2 \, dt \quad (9)$$

where, with a slight abuse of notation, we have denoted the CLF by the same symbol Λ used in (6). Setting to zero the first partial derivative of $\Lambda(\tilde{\mathbf{a}}, \tilde{\mathbf{b}}, \tilde{h}, \tilde{\tau})$ with respect to $\tilde{h}$, and solving for $\tilde{h}$ yields

$$\tilde{h} = \frac{\left| \int_0^{T_0} r(t)\tilde{s}^*(t - \tilde{\tau})dt \right|}{\int_0^{T_0} |\tilde{s}(t - \tilde{\tau})|^2 \, dt} \quad (10)$$

which, used in (9), produces the concentrated likelihood function for the estimation of $\mathbf{a}$, $\mathbf{b}$, and τ, in the form

$$\Lambda(\tilde{\mathbf{a}}, \tilde{\mathbf{b}}, \tilde{\tau}) = \frac{\left| \int_0^{T_0} r(t)\tilde{s}^*(t - \tilde{\tau})dt \right|^2}{\int_0^{T_0} |\tilde{s}(t - \tilde{\tau})|^2 \, dt} \quad (11)$$

The maximization of $\Lambda(\tilde{\mathbf{a}}, \tilde{\mathbf{b}}, \tilde{\tau})$ with respect to $\tilde{\mathbf{a}}$, $\tilde{\mathbf{b}}$, and $\tilde{\tau}$, proves to be intractable, and we are forced to make some approximations by dropping the integral at the denominator of (11). In principle this would be allowed only if it were independent of all the unknown parameters. Actually, it depends on $\tilde{\mathbf{a}}$, $\tilde{\mathbf{b}}$, and $\tilde{\tau}$, but the dependence becomes increasingly weaker with longer observation intervals, as is shown in the Appendix. This means that the approximation is asymptotically correct in the limit as T_0 goes to infinity. The effects of this approximation will be discussed in more detail later, but we expect that doing so will result in the generation

of *data-dependent noise* [17]. Dropping the above integral, the likelihood function then reads

$$\Lambda(\tilde{\mathbf{a}},\tilde{\mathbf{b}},\tilde{\tau}) \approx \left| \int_0^{T_0} r(t)\tilde{s}^*(t-\tilde{\tau})dt \right|^2 \tag{12}$$

Substituting (4) into (12) yields

$$\Lambda(\tilde{\mathbf{a}},\tilde{\mathbf{b}},\tilde{\tau}) = \left| \sum_i \tilde{a}_i X_i(\tilde{\tau}) - j\sum_i \tilde{b}_i X_{i+1/2}(\tilde{\tau}) \right|^2 \tag{13}$$

where

$$X_i(\tilde{\tau}) = \int_0^{T_0} r(t)g(t-\tilde{\tau}-iT)dt \tag{14}$$

and

$$X_{i+1/2}(\tilde{\tau}) = \int_0^{T_0} r(t)g(t-\tilde{\tau}-T/2-iT)dt \tag{15}$$

From the above equations it is evident that $X_i(\tilde{\tau})$ and $X_{i+1/2}(\tilde{\tau})$ can be viewed as the matched filter responses, at the instants $\tilde{\tau}+iT$ and $\tilde{\tau}+T/2+iT$, respectively, to the signal received in the interval $[0, T_0)$.

A preliminary observation is now in order before approaching the maximization of $\Lambda(\tilde{\mathbf{a}},\tilde{\mathbf{b}},\tilde{\tau})$. As it is seen from (13), neither a lower nor an upper limit has been specified for the summation index i because, in principle, it ranges from $-\infty$ to $+\infty$. Actually, if $g(t)$ is assumed to have a finite duration D_gT, with $D_g \in \mathbb{N}$, it can be easily shown that the summations in (13) can be limited to only $L_0 + D_g$ terms. In addition, if we take $g(t)$ causal, (13) becomes

$$\Lambda(\tilde{\mathbf{a}},\tilde{\mathbf{b}},\tilde{\tau}) = \left| \sum_{i=-D_g}^{L_0-1} \tilde{a}_i X_i(\tilde{\tau}) - j\sum_{i=-D_g}^{L_0-1} \tilde{b}_i X_{i+1/2}(\tilde{\tau}) \right|^2 \tag{16}$$

Henceforth, without loss of generality we focus on (16). To proceed further, we assume that $\tilde{\tau}$ is fixed, and we consider the maximization of $\Lambda(\tilde{\mathbf{a}},\tilde{\mathbf{b}},\tilde{\tau})$ with respect to $\tilde{\mathbf{a}},\tilde{\mathbf{b}}$. Despite its apparent exponential complexity, this task can be efficiently performed by resorting to the Mackenthun's algorithm [15] (a similar algorithm can also be found in [18]).

Mackenthun's algorithm solves the following problem: Find the sequence of M-PSK symbols $c_k = e^{j\phi_k}$, with $\phi_k \in \{0, 2\pi/M, \ldots, 2\pi(M-1)/M\}$, that maximizes the function

$$\eta(c_0,\ldots,c_{P-1}) = \left| \sum_{k=0}^{P-1} c_k^* y_k \right|^2 \tag{17}$$

where the y_k are given complex numbers. Setting

$$\begin{aligned} c_{2i} &= \tilde{a}_{-D_g+i} \\ c_{2i+1} &= \tilde{b}_{-D_g+i} \end{aligned} \tag{18}$$

and

$$\begin{aligned} y_{2i} &= X_{-D_g+i}(\tilde{\tau}) \\ y_{2i+1} &= -jX_{-D_g+i+1/2}(\tilde{\tau}) \end{aligned} \tag{19}$$

for $i = 0, 1, \ldots, L_0 + D_g - 1$, it is evident that (16) has the same form as (17) with $M = 2$ and $P = 2(L_0 + D_g)$.

Mackenthun's algorithm provides two binary antipodal sequences, say $\{\hat{a}_i(\tilde{\tau})\}_{i=-D_g}^{L_0-1}$ and $\{\hat{b}_i(\tilde{\tau})\}_{i=-D_g}^{L_0-1}$, that maximize $\Lambda(\tilde{\mathbf{a}},\tilde{\mathbf{b}},\tilde{\tau})$ for a given value of $\tilde{\tau}$. The concentrated likelihood function for the estimation of τ is finally obtained by replacing in (16) $\tilde{a}_i$ and $\tilde{b}_i$ with $\hat{a}_i(\tilde{\tau})$ and $\hat{b}_i(\tilde{\tau})$, respectively. This yields

$$\Lambda(\tilde{\tau}) = \left| \sum_{i=-D_g}^{L_0-1} \hat{a}_i(\tilde{\tau}) X_i(\tilde{\tau}) - j\sum_{i=-D_g}^{L_0-1} \hat{b}_i(\tilde{\tau}) X_{i+1/2}(\tilde{\tau}) \right|^2 \tag{20}$$

The maximization of (20) with respect to $\tilde{\tau}$ provides the ML estimation of τ as

$$\hat{\tau} = \arg\max_{\tilde{\tau}} \Lambda(\tilde{\tau}). \tag{21}$$

No closed-form expression exists for $\hat{\tau}$. Accordingly, its value must be searched for by resorting to numerical algorithms. This issue will be addressed in the next section.

III. Approximate clock estimation.

In this section we deal with the numerical evaluation of the location of the maximum of $\Lambda(\tilde{\tau})$. Specifically, this is done by first computing $\Lambda(\tilde{\tau})$ over a discrete set of points $\mathcal{T}$. As a result, we obtain a set of Λ-values $\mathcal{L} = \{\Lambda(\tilde{\tau}); \tilde{\tau} \in \mathcal{T}\}$. Then, an estimate of $\hat{\tau}$ is determined in *closed-form* as a function of the elements of $\mathcal{L}$.

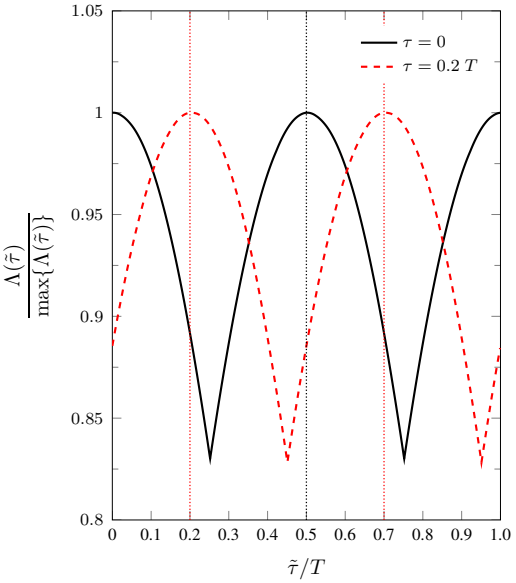

Fig. 1: Typical shapes of $\Lambda(\tilde{\tau})$.

To proceed further, we observe that $\Lambda(\tilde{\tau})$ is an (approximately) $T/2$-periodic function. Indeed, setting $\hat{a}_i(\tilde{\tau}+T/2) = -\hat{b}_i(\tilde{\tau})$ and $\hat{b}_i(\tilde{\tau}+T/2) = -\hat{a}_{i+1}(\tilde{\tau})$ one easily gets

$$\Lambda(\tilde{\tau}+T/2) = \left|jY(\tilde{\tau}) - \hat{a}_{-D_g}(\tilde{\tau})X_{-D_g}(\tilde{\tau})\right|^2 \approx |Y(\tilde{\tau})|^2 = \Lambda(\tilde{\tau})$$

where

$$Y(\tilde{\tau}) = \sum_{i=-D_g}^{L_0-1} \hat{a}_i(\tilde{\tau})X_i(\tilde{\tau}) - j\sum_{i=-D_g}^{L_0-1} \hat{b}_i(\tilde{\tau})X_{i+1/2}(\tilde{\tau})$$

The difference between $\Lambda(\tilde{\tau}+T/2)$ and $\Lambda(\tilde{\tau})$ becomes smaller and smaller as L_0 increases, and it is negligible at all practical values of the observation interval. The periodicity of $\Lambda(\tilde{\tau})$ is also evident from Fig. 1, which shows typical shapes of $\Lambda(\tilde{\tau})$, normalized to the maximum value, obtained with a rolloff factor $\alpha = 0.1$, an observation length of $L_0 = 100$ symbol intervals, and a signal-to-noise ratio $E_s/N_0 = 30$ dB, where $E_s = h^2$. The clock offset τ assumes two different values, namely $\tau = 0$ (solid line) and $\tau = 0.2\ T$ (dashed line). As expected, the maximum of $\Lambda(\tilde{\tau})$ is attained for $\tilde{\tau} = \tau$. The CLF $\Lambda(\tilde{\tau})$ can then be approximated by its Fourier series expansion (FSE) given by

$$\Lambda(\tilde{\tau}) \approx \sum_k \Lambda_k e^{j4\pi k\tilde{\tau}/T} \tag{22}$$

with

$$\Lambda_k \triangleq \frac{2}{T}\int_0^{T/2} \Lambda(\tilde{\tau}) e^{-j4\pi k\tilde{\tau}/T} d\tilde{\tau}. \tag{23}$$

Fig. 2 shows the modulus of Λ_k, for $k = 1, 2, \ldots, 16$. Two different values of the rolloff factor have been considered, namely $\alpha = 0.1$ and $\alpha = 1.0$. It is seen that the amplitude of Λ_k increases with the rolloff, and in both cases the first harmonic is by far the most significant (such a conclusion holds in general, for values of α different than those of Fig. 2). This suggests to approximate $\Lambda(\tilde{\tau})$ by only considering the first harmonic, i.e.,

$$\Lambda(\tilde{\tau}) \approx \Lambda_1 e^{j4\pi\tilde{\tau}/T} + \Lambda_{-1} e^{-j4\pi\tilde{\tau}/T} \tag{24}$$

The validity of the above approximation will be assessed later by computer simulations. Since $\Lambda_1 = \Lambda_{-1}^*$, the maximization of (24) with respect to $\tilde{\tau}$ yields

$$\hat{\tau} = -\frac{\arg\{\Lambda_1\}}{4\pi}\ T + \ell\frac{T}{2} \tag{25}$$

for an arbitrary integer ℓ. Equation (25) shows that the timing estimates are ambiguous by multiples of $T/2$. This is expected in view of the $T/2$ delay between the I and Q signals. Since in the absence of additional information the receiver cannot resolve this ambiguity, without loss of generality we henceforth assume $\hat{\tau} \in [0, T/2)$.

Now, it remains to solve the problem of determining Λ_1. As a first step in this direction, we assume that the summation in (22) can be limited to a finite number of terms as follows

$$\Lambda(\tilde{\tau}) = \sum_{k=-Q/2+1}^{Q/2-1} \Lambda_k e^{j4\pi k\tilde{\tau}/T} \tag{26}$$

where $Q-1$ is the number of significant components in the FSE of $\Lambda(\tilde{\tau})$ (it is assumed that Q is an even integer). Now, consider the Q samples of $\Lambda(\tilde{\tau})$ taken at a rate $Q/(T/2)$ and given by

$$\Lambda\left(m\frac{T}{2Q}\right) = \sum_{k=-Q/2+1}^{Q/2-1} \Lambda_k e^{j2\pi km/Q} \tag{27}$$

for $m = 0, 1, \ldots, Q-1$. From (27) one easily gets

$$\Lambda_1 = \frac{1}{Q}\sum_{m=0}^{Q-1} \Lambda\left(m\frac{T}{2Q}\right) e^{-j2\pi m/Q} \tag{28}$$

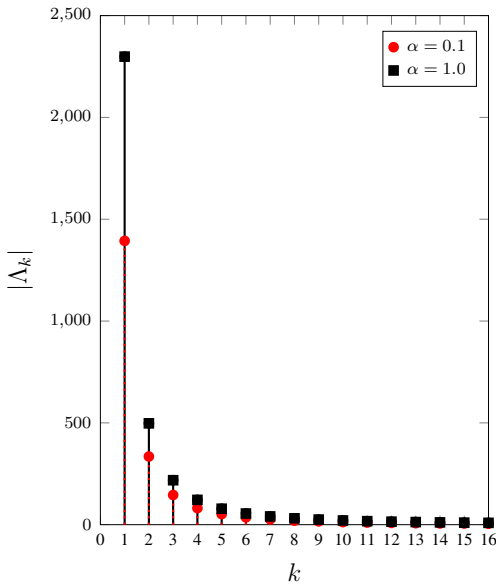

Fig. 2: Modulus of Λ_k for $k = 1, \ldots, 16$. The rolloff factor is $\alpha = 0.1$ or $\alpha = 1.0$.

which provides Λ_1 as a function of the elements of the set $\mathcal{L} = \{\Lambda(\tilde{\tau}); \tilde{\tau} \in \mathcal{T}\}$ with $\mathcal{T} = \{mT/2Q; m = 0, \ldots, Q-1\}$.

After that $\hat{\tau}$ has been computed using (25), the value of θ is estimated as follows. We first apply Mackenthun's algorithm in order to determine the binary sequences $\hat{\mathbf{a}} = \{\hat{a}_i\}_{i=-D_g}^{L_0-1}$ and $\hat{\mathbf{b}} = \{\hat{b}_i\}_{i=-D_g}^{L_0-1}$, that maximize (16) with $\tilde{\tau} = \hat{\tau}$. Then, an estimate of θ is found through (8) by evaluating $\vartheta(\tilde{\mathbf{a}}, \tilde{\mathbf{b}}, \tilde{\tau})$ at $\tilde{\mathbf{a}} = \hat{\mathbf{a}}$, $\tilde{\mathbf{b}} = \hat{\mathbf{b}}$, and $\tilde{\tau} = \hat{\tau}$, i.e.,

$$\hat{\theta} = \vartheta(\hat{\mathbf{a}}, \hat{\mathbf{b}}, \hat{\tau}). \tag{29}$$

A final remark is now in order. It can be shown that, for a fixed value of $\hat{\tau}$, the phase estimates provided by (29) are ambiguous by multiples of π. This is evident by observing that both the pairs $(\hat{\mathbf{a}}, \hat{\mathbf{b}})$ and $(-\hat{\mathbf{a}}, -\hat{\mathbf{b}})$ maximize $\Lambda(\tilde{\mathbf{a}}, \tilde{\mathbf{b}}, \hat{\tau})$, and hence $\hat{\theta} = \vartheta(\hat{\mathbf{a}}, \hat{\mathbf{b}}, \hat{\tau})$ and $\hat{\theta} \pm \pi = \vartheta(-\hat{\mathbf{a}}, -\hat{\mathbf{b}}, \hat{\tau})$ are both valid phase estimates. The differential enconding/decoding scheme discussed in [14, Sect. 8.6] can be used to resolve such ambiguities.

A. *Implementation issues.*

i) The value of Q comes from a trade-off between performance and complexity. Indeed, on the one hand we expect that increasing Q may result in a better approximation of $\Lambda(\tilde{\tau})$ in (26), and hence in better performance. On the other hand, the greater Q the higher the implementation complexity. Fig. 3 shows the timing mean-squared estimation error (MSEE) as a function of Q, for two different values of the rolloff parameter, namely $\alpha = 0.1$ and $\alpha = 1.0$. The observation length is $L_0 = 100$, and the SNR is either $E_s/N_0 = 10$ dB or $E_s/N_0 = 30$ dB. It is seen that, for both values of α and E_s/N_0, MSEE reduces as Q increases, as expected. Notice, however, that only marginal improvements are observed when Q grows above 8. Accordingly, in the following it is assumed $Q = 8$ for the sake of complexity.

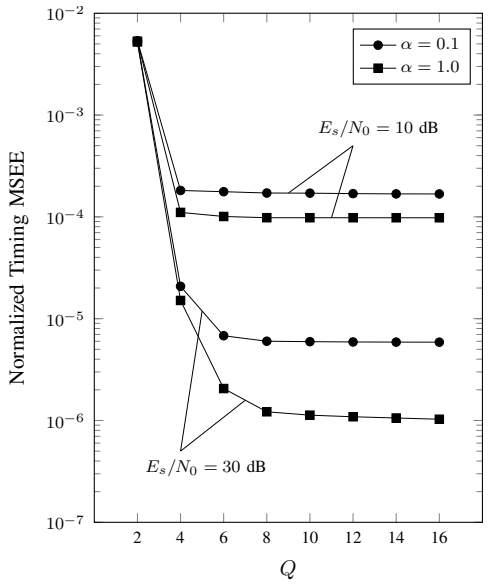

Fig. 3: Normalized timing MSEE as a function of Q, for two different values of E_s/N_0 and two different values of α. The observation length is $L_0 = 100$.

ii) Inspection of (20) reveals that the computation of $\Lambda(mT/2Q)$, for $m = 0, \ldots, Q-1$, requires $X_i(mT/2Q)$ and $X_{i+1/2}(mT/2Q)$. In principle, they can be obtained by sampling the output of the matched filter at a rate $2Q/T$, as indicated by (14) and (15). The main drawback of this solution may be the power consumption of the analog-to-digital converter (ADC) due to its quite high sampling rate [19]. Various alternative schemes, with a sampling rate lower than $2Q/T$, can be devised for generating $X_i(mT/2Q)$ and $X_{i+1/2}(mT/2Q)$. A possible architecture, that has been used for assessing the performance of the proposed algorithm, is depicted in Fig. 4. Here, the received waveform is first passed through an anti-aliasing filter (AAF), and then it is sampled at a rate $1/T_s = N/T$, with $N = 2Q/M$ (both N and M are assumed integers). The zero-padding block inserts $M-1$ zeros between two consecutive samples, and hence the output rate is exactly $2Q/T$. The resulting sequence $r_{ZP}[k]$ is finally passed through a digital matched-filter $g[-k] \triangleq g(-kT/2Q)$ which produces $x[k]$. It can easily be shown that

$$x[k] = \int_0^{T_0} r(t) g(t - kT/2Q) dt \tag{30}$$

so that

$$X_i(mT/2Q) = x[m + 2Qi] \tag{31}$$

and

$$X_{i+1/2}(mT/2Q) = x[m + Q + 2Qi] \tag{32}$$

iii) The estimation of θ through (29) requires the computation of $X_i(\hat{\tau})$ and $X_{i+1/2}(\hat{\tau})$, which can be obtained from the sequence $r[n]$ at the output of the sampling device in the following way:

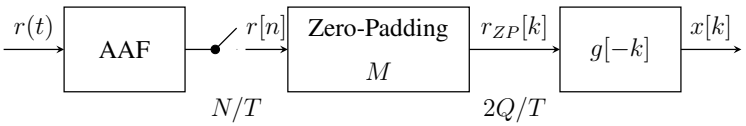

Fig. 4: Generation of $X_i(\tilde{\tau})$ and $X_{i+1/2}(\tilde{\tau})$.

$$X_i(\hat{\tau}) = \sum_{n=0}^{NL_0-1} r[n] g_{\hat{\tau}}[n - iN] \tag{33}$$

and

$$X_{i+1/2}(\hat{\tau}) = \sum_{n=0}^{NL_0-1} r[n] g_{\hat{\tau}}[n - N/2 - iN] \tag{34}$$

where $g_{\hat{\tau}}[n] \triangleq g(nT/N - \hat{\tau})$. Clearly, this also requires storing the sequence $r[n]$.

A different estimate of θ can be obtained by approximating $\vartheta(\hat{\mathbf{a}}, \hat{\mathbf{b}}, \hat{\tau})$ in (29) as follows. During the timing estimation step, the quantities $\Lambda(mT/2Q) = |Y_m|^2$ with

$$\begin{aligned} Y_m = &\sum_{i=-D_g}^{L_0-1} \hat{a}_i(mT/2Q) X_i(mT/2Q) \\ &-j \sum_{i=-D_g}^{L_0-1} \hat{b}_i(mT/2Q) X_{i+1/2}(mT/2Q) \end{aligned} \tag{35}$$

are computed for $m = 0, 1, \ldots, Q-1$. This means that, at the end of clock estimation, Y_m is available along with $\Lambda(mT/2Q)$. Accordingly, $\vartheta(\hat{\mathbf{a}}, \hat{\mathbf{b}}, \hat{\tau})$ can be approximated by $\arg\{Y_{\widehat{m}}\}$, where $\widehat{m}$ is the value of the index m corresponding to the minimum distance between $mT/2Q$ and $\hat{\tau}$ (with the distance being measured modulo $T/2$). The resulting phase estimator then reads

$$\hat{\theta}_a = \arg\{Y_{\widehat{m}}\} \tag{36}$$

Clearly, the estimation of the phase by (36) requires neither additional computational costs (apart the computation of the argument of a complex number) nor storing the sequence $r[n]$.

B. Computational complexity.

We now evaluate the computational complexity of the proposed estimators.

1) Timing Estimation: We start with the computation of $\Lambda(mT/2Q)$ through (20). This requires:

a) Computing $X_i(mT/2Q)$ and $X_{i+1/2}(mT/2Q)$, for $i = -D_g, \ldots, L_0 - 1$. Since $2(D_g N + 1)$ real multiplications and $2D_g N$ real additions are necessary for the evaluation of $X_i(mT/2Q)$ as well as of $X_{i+1/2}(mT/2Q)$, a total of $4(D_g N + 1)(L_0 + D_g)$ real multiplications and $4D_g N(L_0 + D_g)$ real additions are needed for this step;

b) Applying Mackenthun's algorithm for the computation of $\{\hat{a}_i(mT/2Q), \hat{b}_i(mT/2Q)\}_{i=-D_g}^{L_0-1}$. Based on the results in [15], this requires:

- Sorting $2(L_0 + D_g)$ complex numbers according to their phases;

- $12(L_0 + D_g) - 6$ real additions;
- Computing the squared magnitude of $2(L_0 + D_g)$ complex numbers. This amounts to $4(L_0 + D_g)$ real multiplications and $2(L_0 + D_g)$ real additions.

Once $\Lambda(mT/2Q)$ has been computed for $m = 0, 1, \ldots, Q-1$, Λ_1 is evaluated through (28). This step requires no more than $4Q$ real multiplications and $2(2Q - 1)$ real additions.

Finally, estimating τ by (25) requires the computation of the argument of Λ_1, and a real multiplication.

2) Phase Estimation through (29)*:* From the results of the previous section, it can easily be shown that the computation of (29) requires:

- $2(2D_gN + 7)(L_0 + D_g) - 6$ real additions;
- $4(D_gN + 2)(L_0 + D_g)$ real multiplications;
- Sorting $2(L_0 + D_g)$ complex numbers according to their phases;
- Computing the argument of a complex number.

3) Phase Estimation through (36)*:* In this case only the computation of the argument of a complex number is required.

We now evaluate the computational complexity of the feedforward joint clock and phase estimator proposed in [12], henceforth referred to as DDM-EST. Assuming an oversampling factor of $N = 2$ (as suggested in [12]), it is easily found that DDM-EST requires: *i*) $8NL_0(ND+1)-2$ real additions; *ii*) $4NL_0(2ND + 3) + 2$ real multiplications; *iii*) computing the argument of 2 complex numbers. Parameter D is half the duration (in symbol intervals) of the pulse $q(t)$ whose Fourier transform is given in [12, Eq. (16)].

The total number of real additions and multiplications for the joint timing and phase estimators proposed in this paper are summarized in the first two rows of Table I. In the third row, the same quantities are shown for DDM-EST. As an example, Table II reports the total number of operations for each estimator assuming $N = 2$, $D_g = 2D = 16$, $Q = 8$, and $L_0 = 50$. It is worth noticing that the results in Table II do not take into account the complexity due to sorting in Mackenthun's algorithm, which requires a number of operations on the order of $2Q(L_0+D_g)[1+\log_2(L_0+D_g)]$.

IV. Simulation results

The performance of the synchronization algorithms described in the previous sections has been assessed by simulation and compared with that of other clock/phase estimators proposed in literature. We have used the mean squared error of the estimates (MSEE) as performance metric. An oversampling factor $N = 4$ has been adopted, whereas $g(t)$ has a root-raised cosine Fourier transform with rolloff α and duration $D_g = 16$ symbol intervals.

Fig. 5 shows the mean squared error of the clock estimates normalized to the symbol period T, as a function of E_s/N_0. The rolloff parameter is $\alpha = 0.1$, and the observation length (in symbol intervals) is either $L_0 = 50$ or $L_0 = 300$. Circular marks indicate simulation results whereas the thin solid lines are drawn to ease the reading. The square marks in Fig. 5 are for the MSEE obtained by maximizing (20) instead of (24). It is seen that approximating $\Lambda(\tilde{\tau})$ through (24) does not produce any significant performance loss, for neither $L_0 = 50$ nor $L_0 = 300$. As we shall see soon, the same conclusions hold for $\alpha = 1.0$ as well, meaning that (24) is a sensible approximation of $\Lambda(\tilde{\tau})$ as far as the estimation of τ is concerned. The straight thick solid lines represent the modified Cramér-Rao bounds (MCRBs) discussed in [20]. They are given by

$$\frac{1}{T^2}\mathrm{MCRB}_\tau = \frac{1}{8\pi^2\xi L_0}\frac{1}{E_s/N_0} \tag{37}$$

with

$$\xi = \frac{1}{12} + \alpha^2\left(\frac{1}{4} - \frac{2}{\pi^2}\right). \tag{38}$$

Notice that ξ is an increasing function of α, and hence MCRB_τ decreases as the rolloff increases. This means that the best estimation performance is to be expected for the highest values of α. As can be seen from Fig. 5, the performance of the timing estimator is very close to the theoretical limits provided by (37) at SNR values in the range $(7.5, 20)$ dB, for both $L_0 = 50$ and $L_0 = 300$. This means that a good estimation accuracy can be achieved even with quite short observation intervals and small values of α. At low and high SNRs ($E_s/N_0 < 5$ dB and $E_s/N_0 > 25$ dB, respectively) the MSEE curves depart from the MCRB. In the former case, the loss with respect to the limit (37) can be explained with the fact that, as it is well known, MCRB is quite loose at low signal-to-noise ratios or when the number of observed data is small. In the latter case, it is probably due to approximating the true likelihood function (11) by (12). This can be proved indirectly, by observing that, in the absence of noise, the *true* set of parameters h, θ, τ, $\mathbf{a}$, and $\mathbf{b}$, maximizes the likelihood function (3). This means that, if no approximation were introduced, the MSEEs would tend to zero as the signal-to-noise ratio increases. Since it has already been shown that approximating (20) with (24) has no impact on the MSEE, it can be concluded that the floor in the MSEE curves, which is visible at high SNRs, is due to the use of (12) in place of of the true likelihood function (11). Evidence of the fact that dropping the integral at the denominator of (11) results in data-dependent noise (also called *pattern-dependent jitter* or *self-noise* [21]) can be found, for example, in [17] and [14, Section 7.4]. Notice that the approximation of the true likelihood function (11) by (12) is more and more accurate as the observation length L_0 increases, as is shown in the Appendix. Indeed, the gap between the MSEE curves and the relevant MCRBs reduces in passing from $L_0 = 50$ to $L_0 = 300$. Finally, the straight dotted line in Fig. 5 shows the Cramér-Rao bounds for clock estimation as obtained by assuming a known training sequence and *QPSK symbols*. In particular, an "alternating" pilot pattern has been chosen, i.e., $a_i = (-1)^i$ and $b_i = (-1)^i$. In [22] it has been shown that such a sequence is optimal for the joint estimation of τ and θ[1]. With the above choice, it is found [23]

$$\frac{1}{T^2}\mathrm{CRB}_\tau = \frac{1}{2\pi^2 L_0}\frac{1}{E_s/N_0} \tag{39}$$

CRB_τ allows us to measure the performance loss of the proposed estimator with respect to an efficient *data-aided* clock estimator. This loss depends on the rolloff factor, since CRB_τ

[1]To the best of our knowledge, the problem of optimizing the training symbols for OQPSK constellations has not been solved yet.

TABLE I: Complexity of the investigated schemes.

Algorithm	Real Additions	Real Multiplications
(25) and (29)	$2(Q+1)(2D_gN+7)(L_0+D_g)-2Q-8$	$4(Q+1)(D_gN+2)(L_0+D_g)+4Q+1$
(25) and (36)	$2Q(2D_gN+7)(L_0+D_g)-2Q-2$	$4Q(D_gN+2)(L_0+D_g)+4Q+1$
DDM-EST	$8NL_0(ND+1)-2$	$4NL_0(2ND+3)+2$

TABLE II: Computational complexity for $N=2$, $D_g=2D=16$, $Q=8$, and $L_0=50$

Algorithm	Real Additions	Real Multiplications
(25) and (29)	84324	80817
(25) and (36)	74958	71841
DDM-EST	13598	14002

does not depend on α, differently from MCRB_τ. In particular, the ratio $\mathrm{MCRB}_\tau/\mathrm{CRB}_\tau$ attains its maximum value of 3 for $\alpha=0$; the minimum is equal to $0.75/(1-6/\pi^2)<2$, and is achieved for $\alpha=1$. Since the gap between MCRB_τ and CRB_τ does not depend on L_0, in Fig. 5 CRB_τ has been reported only for $L_0=300$, in order not to crowd the figure.

Fig. 6 illustrates the phase MSEE as a function of E_s/N_0. The simulation parameters are the same as in Fig. 5. The performance of the proposed algorithm is compared with the MCRB given by

$$\mathrm{MCRB}_\theta=\frac{1}{2L_0}\frac{1}{E_s/N_0} \tag{40}$$

As can be seen, the phase MSEE curves follow the same trend as the corresponding curves in Fig. 5, and they are very close to or coincide with the MCRB in a wide range of SNRs. It is worth noticing that the Cramér-Rao bound for the phase estimation corresponding to the "alternating" training sequence considered above coincides with MCRB_θ, as can be easily shown by using the results in [23].

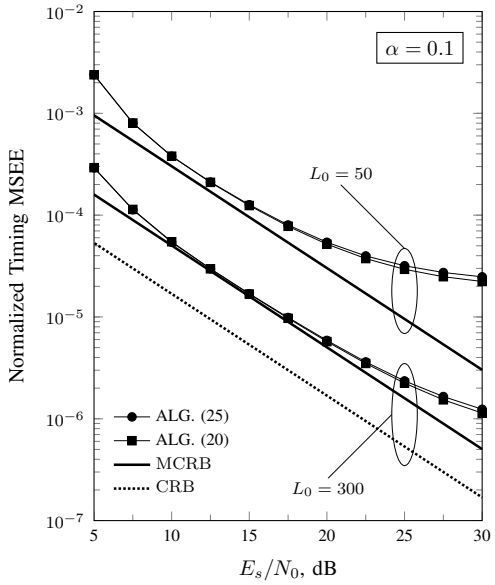

Fig. 5: Normalized timing MSEE versus E_s/N_0 for $\alpha=0.1$ and two different values of the observation length, $L_0=50$ and $L_0=300$.

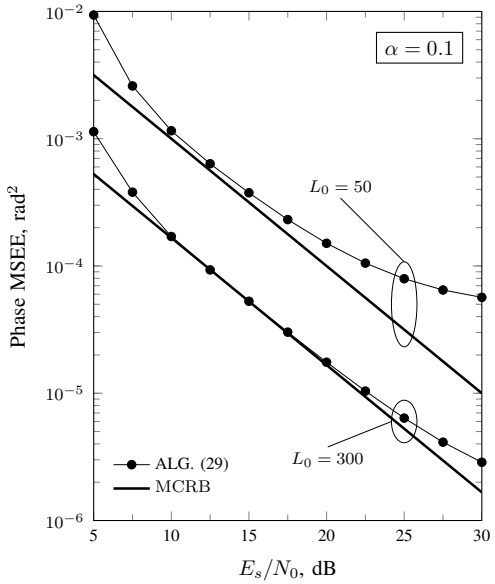

Fig. 6: Phase MSEE versus E_s/N_0 for $\alpha=0.1$ and two different values of the observation length, $L_0=50$ and $L_0=300$.

Fig. 7 and Fig. 8 show the MSEE for clock and phase, respectively, with $\alpha=1.0$. The observation length is either $L_0=50$ or $L_0=300$. As expected, both the clock and phase estimators have improved performance compared to the case $\alpha=0.1$. In particular, the MSEEs coincide with the relevant MCRBs with both $L_0=50$ and $L_0=300$ at almost all the considered SNR values. Contrasting the curves of Fig. 5 and Fig. 7, it can be observed that, for a given observation length L_0, the gap between the MSEE curves and the relevant MCRBs reduces in passing from $\alpha=0.1$ to $\alpha=1.0$. This is due to the fact that the error in approximating (11) by (12) decreases as the rolloff increases, as it could be inferred from the results in the Appendix.

It is interesting to compare the performance of the present estimators with that of other schemes already proposed in literature. We first focus on clock estimation, and we consider two synchronization schemes with a lower complexity compared to (25). The first is the feedforward joint clock and phase estimator DDM-EST, proposed and analyzed in [12]. The second is the closed-loop estimator suggested by Gardner in [10] and also described in [14], where it is denoted as I/Q-GAD. Fig. 9 shows the normalized timing MSEE with $\alpha=0.25$. The observation length is $L_0=100$ for both the feedforward schemes considered in the figure, namely (25) and DDM-EST. The normalized bandwidths are $B_\tau T=5\times10^{-3}$ and $B_\theta T=5\times10^{-3}$ for the I/Q-GAD clock and phase loops (see [14]), respectively. They are equivalent to an observation interval of $L_0=100$ symbols, in a feedforward scheme. It is

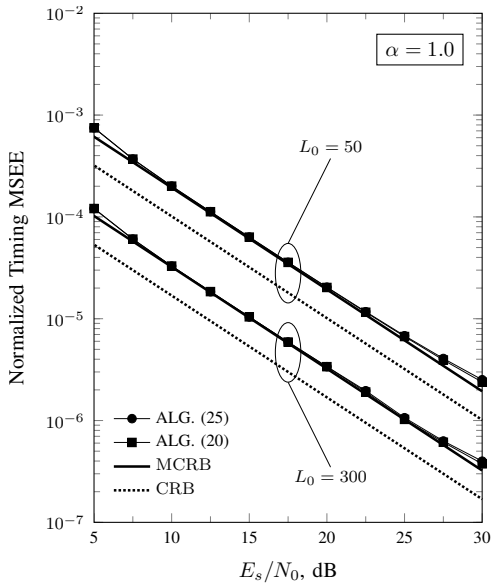

Fig. 7: Normalized timing MSEE versus E_s/N_0 for $\alpha = 1.0$ and two different values of the observation length, $L_0 = 50$ and $L_0 = 300$.

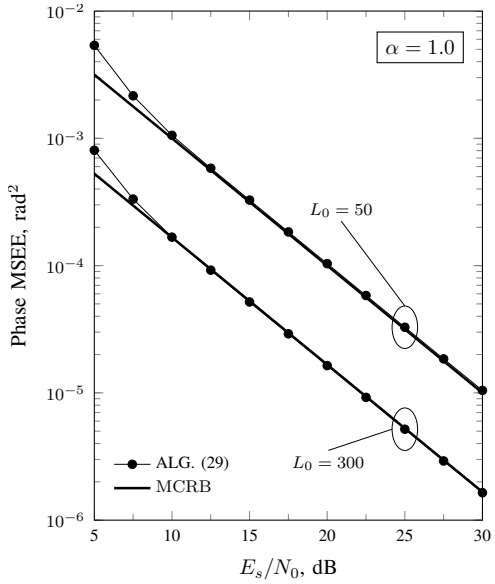

Fig. 8: Phase MSEE versus E_s/N_0 for $\alpha = 1.0$ and two different values of the observation length, $L_0 = 50$ and $L_0 = 300$.

seen that estimator (25) largely outperforms both DDM-EST and I/Q-GAD at all SNRs, and its performance is very close to the MCRB. On the other hand, the superiority of the proposed estimator becomes less marked as the rolloff increases. This is evident from the results shown in Fig. 10 where the MSEE of (25) is compared with that of DDM-EST and I/Q-GAD for $\alpha = 0.75$. The other simulation parameters are the same as in Fig. 9.

Now, we turn our attention on phase estimation. Fig. 11 shows the MSEEs of (29), (36), and DDM-EST, with $\alpha = 0.25$ and $L_0 = 100$. In addition, the curve MA-EST illustrates simulation results obtained with the *clock-aided* phase estimator proposed by Moeneclaey and Ascheid in [11]. This algorithm operates on the samples $X_i(\tau)$ and $X_{i+1/2}(\tau)$ at the output of the matched filter taken at the instants $iT + \tau$ and $iT + T/2 + \tau$, respectively. This means that clock information must be already available. The phase is estimated as

$$\hat{\theta}_{MA} = \frac{1}{2} \arg \left\{ \sum_{i=0}^{L_0-1} \left[e^{j2 \arg[X_i(\tau)]} - e^{j2 \arg[X_{i+1/2}(\tau)]} \right] \right\} \tag{41}$$

It is seen that both (29) and (36) have considerably better performance than DDM-EST and MA-EST at all SNRs. Also, the loss of the approximate ML estimator (36) with respect to (29) is negligible for $E_s/N_0 < 25$ dB.

Finally, Fig. 12 shows the effects of estimation errors on the bit error rate (BER) performance. Specifically, in order to cope with the ambiguities of the clock and phase estimates we have considered the differential encoder illustrated in [14, Sect. 8.6]. Once τ and θ have been estimated, a coherent detection scheme (with a two-symbols observation interval) have been used for decoding the differentially encoded bits [24], [25]. The rolloff factor is $\alpha = 0.1$, and the observation interval for clock and phase estimation is $L_0 = 50$. Circular marks show the bit error rate as a function of $E_b/N_0 = h^2/2N_0$, when the clock and phase estimates are provided by (25) and (29), respectively. Square marks are for the BER performance obtained by using DDM-EST (but identical results have been found with the clock and phase estimator described in [13]). The thick curve represents the BER of an ideal system with no estimation errors. It is given by

$$\mathrm{BER}_{id} = 2Q\left(\sqrt{\frac{2E_b}{N_0}}\right)\left[1 - Q\left(\sqrt{\frac{2E_b}{N_0}}\right)\right] \tag{42}$$

where function $Q(\cdot)$ is the tail probability of a standard normal distribution. From the results in Fig. 12, it is seen that the proposed estimator largely outperforms the conventional synchronizers also in terms of BER (at least, for small rolloff factors and short observation intervals). In addition, it virtually provides the same BER performance as an ideal system with no estimation errors.

V. Conclusions

We have proposed feedforward algorithms for phase and timing recovery in OQPSK modulations. They have been derived by ML arguments, and can be implemented in digital form. The performance of the resulting schemes is very good and close to the theoretical limits provided by the MCRB. Accurate estimation is possible even with relatively short observation intervals and small excess bandwidths. Compared to other algorithms already known in literature the proposed estimators have remarkably better performance, at the price of a higher computational complexity. Though they have been proposed for offset modulation formats, our schemes can be extended to conventional PSK signals (with an arbitrary dimension of the symbol constellation).

Appendix

In this appendix, we show that the denominator in (11) can be written as the sum of a term independent of $\tilde{\mathbf{a}}$, $\tilde{\mathbf{b}}$, and

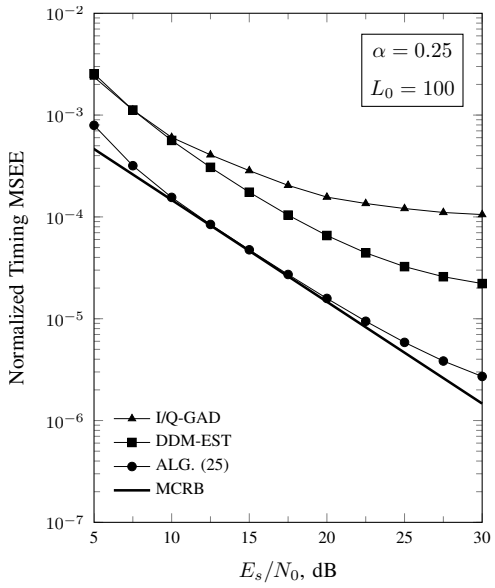

Fig. 9: Normalized timing MSEE versus E_s/N_0 with $\alpha = 0.25$ and $L_0 = 100$.

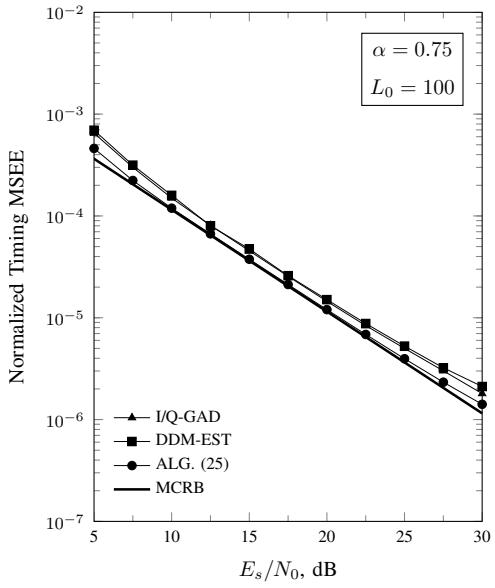

Fig. 10: Normalized timing MSEE versus E_s/N_0 with $\alpha = 0.75$ and $L_0 = 100$.

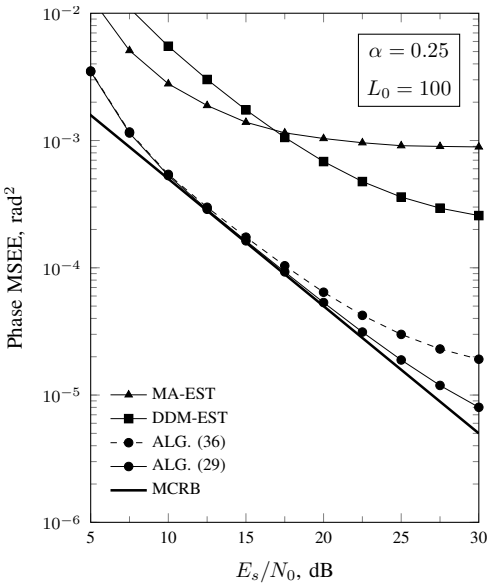

Fig. 11: Phase MSEE versus E_s/N_0 with $\alpha = 0.25$ and $L_0 = 100$.

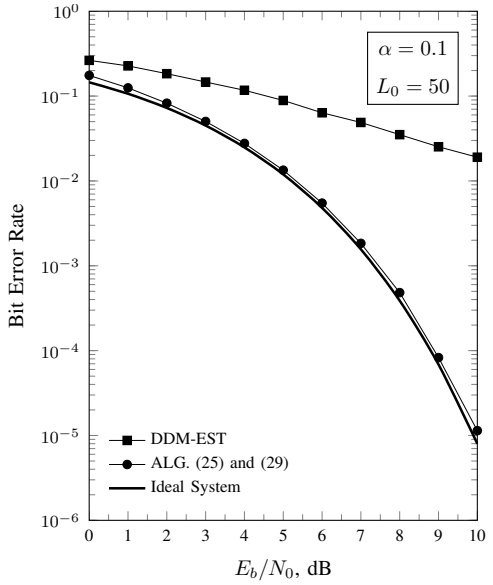

Fig. 12: Bit Error Rate versus E_b/N_0 with $\alpha = 0.1$ and $L_0 = 50$.

$\tilde{\tau}$, and whose value increases linearly with the observation length L_0, and other terms which depend on $\tilde{\mathbf{a}}$, $\tilde{\mathbf{b}}$, and $\tilde{\tau}$, but whose values are independent of L_0, and do not change with the observation interval. This means that the contribution of such terms becomes more and more marginal as L_0 increases, and hence $\int_0^{T_0} |\tilde{s}(t-\tilde{\tau})|^2 \, dt$ becomes asymptotically (i.e. in the limit as L_0 goes to infinity) independent of $\tilde{\mathbf{a}}$, $\tilde{\mathbf{b}}$, and $\tilde{\tau}$. Henceforth, it is assumed that $g(t)$ has a root-raised-cosine Fourier transform with rolloff α.

We start by writing the denominator in (11) as follows:

$$\int_0^{T_0} |\tilde{s}(t-\tilde{\tau})|^2 \, dt = \int_{-\tilde{\tau}}^{0} |\tilde{s}(t)|^2 \, dt + \int_0^{T_0-T} |\tilde{s}(t)|^2 \, dt + \int_{T_0-T}^{T_0-\tilde{\tau}} |\tilde{s}(t)|^2 \, dt \tag{43}$$

which shows that the left-hand side of (43) is the sum of three terms, one of which (the central term at the right-hand side) is independent of $\tilde{\tau}$, and is clearly the most significant, as we shall soon see. We first focus on this term. Taking (4) into account, it is found that $\int_0^{T_0-T} |\tilde{s}(t)|^2 \, dt$ can be written as

$$\int_0^{T_0-T} |\tilde{s}(t)|^2 \, dt = 2(L_0-1)E_g + A(\tilde{\mathbf{a}}', \tilde{\mathbf{a}}'') + B(\tilde{\mathbf{b}}', \tilde{\mathbf{b}}'') \tag{44}$$

where

$$A(\tilde{\mathbf{a}}',\tilde{\mathbf{a}}'') = \sum_{\substack{i,k=-D_g+1\\ i\neq k}}^{-1} \tilde{a}_i\tilde{a}_k \int_0^{T_0-T} g(t-iT)g(t-kT)dt + \sum_{\substack{i,k=L_0-D_g\\ i\neq k}}^{L_0-2} \tilde{a}_i\tilde{a}_k \int_0^{T_0-T} g(t-iT)g(t-kT)dt \tag{45}$$

$$B(\tilde{\mathbf{b}}',\tilde{\mathbf{b}}'') = \sum_{\substack{i,k=-D_g\\ i\neq k}}^{-1} \tilde{b}_i\tilde{b}_k \int_0^{T_0-T} g(t-T/2-iT)g(t-T/2-kT)dt + \sum_{\substack{i,k=L_0-D_g-1\\ i\neq k}}^{L_0-2} \tilde{b}_i\tilde{b}_k \int_0^{T_0-T} g(t-T/2-iT)g(t-T/2-kT)dt \tag{46}$$

$\tilde{\mathbf{a}}' = \{\tilde{a}_i(\tilde{\tau})\}_{i=-D_g}^{-1}$, $\tilde{\mathbf{a}}'' = \{\tilde{a}_i(\tilde{\tau})\}_{i=L_0-D_g}^{L_0-1}$, $\tilde{\mathbf{b}}' = \{\tilde{b}_i(\tilde{\tau})\}_{i=-D_g}^{-1}$, and $\tilde{\mathbf{b}}'' = \{\tilde{b}_i(\tilde{\tau})\}_{i=L_0-D_g-1}^{L_0-1}$. From (45)-(46) it is seen that $A(\tilde{\mathbf{a}}',\tilde{\mathbf{a}}'')$ and $B(\tilde{\mathbf{b}}',\tilde{\mathbf{b}}'')$ depend only on the first and the last D_g symbols of the trial sequences $\tilde{\mathbf{a}}$ and $\tilde{\mathbf{b}}$, but they do not depend on the *central* symbols. Also, more importantly, $A(\tilde{\mathbf{a}}',\tilde{\mathbf{a}}'')$ and $B(\tilde{\mathbf{b}}',\tilde{\mathbf{b}}'')$ do not depend on the length L_0 of the observation interval. This means that they become increasingly less important compared to the term $2(L_0-1)E_g$ as L_0 grows.

Now we turn attention to the terms depending on $\tilde{\tau}$ in (43). Simple calculations show that the following relationships hold:

$$\int_{-\tilde{\tau}}^{0} |\tilde{s}(t)|^2\,dt + \int_{T_0-T}^{T_0-\tilde{\tau}} |\tilde{s}(t)|^2\,dt = 2E_g + C(\tilde{\mathbf{a}}',\tilde{\mathbf{a}}'',\tilde{\tau}) + D(\tilde{\mathbf{b}}',\tilde{\mathbf{b}}'',\tilde{\tau}) \tag{47}$$

where

$$C(\tilde{\mathbf{a}}',\tilde{\mathbf{a}}'',\tilde{\tau}) = \sum_{\substack{i,k=-D_g\\ i\neq k}}^{-1} \tilde{a}_i\tilde{a}_k \int_{-\tilde{\tau}}^{0} g(t-iT)g(t-kT)dt + \sum_{\substack{i,k=L_0-D_g\\ i\neq k}}^{L_0-1} \tilde{a}_i\tilde{a}_k \int_{T_0-T}^{T_0-\tilde{\tau}} g(t-iT)g(t-kT)dt \tag{48}$$

$$D(\tilde{\mathbf{b}}',\tilde{\mathbf{b}}'',\tilde{\tau}) = \sum_{\substack{i,k=-D_g\\ i\neq k}}^{-1} \tilde{b}_i\tilde{b}_k \int_{-\tilde{\tau}}^{0} g(t-T/2-iT)g(t-T/2-kT)dt + \sum_{\substack{i,k=L_0-D_g-1\\ i\neq k}}^{L_0-1} \tilde{b}_i\tilde{b}_k \int_{T_0-T}^{T_0-\tilde{\tau}} g(t-T/2-iT)g(t-T/2-kT)dt \tag{49}$$

Replacing (44) and (47) into (43) yields

$$\int_0^{T_0} |\tilde{s}(t-\tilde{\tau})|^2\,dt = 2L_0E_g \times \left[1 + \frac{A(\tilde{\mathbf{a}}',\tilde{\mathbf{a}}'') + B(\tilde{\mathbf{b}}',\tilde{\mathbf{b}}'') + C(\tilde{\mathbf{a}}',\tilde{\mathbf{a}}'',\tilde{\tau}) + D(\tilde{\mathbf{b}}',\tilde{\mathbf{b}}'',\tilde{\tau})}{2L_0E_g}\right] \tag{50}$$

from which, taking into account that $A(\tilde{\mathbf{a}}',\tilde{\mathbf{a}}'')$, $B(\tilde{\mathbf{b}}',\tilde{\mathbf{b}}'')$, $C(\tilde{\mathbf{a}}',\tilde{\mathbf{a}}'',\tilde{\tau})$, and $D(\tilde{\mathbf{b}}',\tilde{\mathbf{b}}'',\tilde{\tau})$, do not vary with L_0, one readily gets

$$\lim_{L_0\to\infty} \int_0^{T_0} |\tilde{s}(t-\tilde{\tau})|^2\,dt = 2L_0E_g \tag{51}$$

The above equation shows that the denominator in (11) is asymptotically (i.e. in the limit as L_0 goes to infinity) independent of $\tilde{\mathbf{a}}$, $\tilde{\mathbf{b}}$, and $\tilde{\tau}$, meaning that the approximation of (11) by (12) becomes more and more accurate as the observation interval increases.

From (50) it is evident that the approximation error can be measured by the ratio $\rho = [A(\tilde{\mathbf{a}}',\tilde{\mathbf{a}}'') + B(\tilde{\mathbf{b}}',\tilde{\mathbf{b}}'') + C(\tilde{\mathbf{a}}',\tilde{\mathbf{a}}'',\tilde{\tau}) + D(\tilde{\mathbf{b}}',\tilde{\mathbf{b}}'',\tilde{\tau})]/2L_0E_g$. For fixed values of $\tilde{\mathbf{a}}'$, $\tilde{\mathbf{a}}''$, $\tilde{\mathbf{b}}'$, $\tilde{\mathbf{b}}''$ and $\tilde{\tau}$, it is seen that ρ depends on the rolloff factor through the integrals in (45), (46), (48) and (49). In particular, simulation results (which have not been reported for limitations of space) indicate that the absolute value of these integrals increases as the rolloff decreases (as expected, since the smaller the rolloff the larger the sidelobes of the root-raised-cosine pulse). Accordingly, it can be guessed that for a given observation length L_0 the approximation error is smaller with higher values of the excess bandwidth. This is confirmed by the results shown in Section IV.

REFERENCES

[1] R. A. Harris, "Transmission Analysis and Design for the ECS System," in *4th International Conference on Digital Satellite Communications*, vol. 1, 1979, pp. 81–93.

[2] L. Lundquist, "Modulation Techniques for Band and Power Limited Satellite Channels," in *4th International Conference on Digital Satellite Communications*, vol. 1, 1979, pp. 94–100.

[3] R. Raich and G. T. Zhou, "Analyzing Spectral Regrowth of QPSK and OQPSK Signals," in *Acoustics, Speech, and Signal Processing, 2001. Proceedings.(ICASSP'01). 2001 IEEE International Conference on*, vol. 4. IEEE, 2001, pp. 2673–2676.

[4] F. M. Gardner, "A BPSK/QPSK Timing-Error Detector for Sampled Receivers," *IEEE Transactions on Communications*, vol. 34, pp. 423–429, 1986.

[5] M. Oerder and H. Meyr, "Digital Filter and Square Timing Recovery," *IEEE Transactions on communications*, vol. 36, no. 5, pp. 605–612, 1988.

[6] A. N. D'Andrea and M. Luise, "Optimization of Symbol Timing Recovery for QAM Data Demodulators," *Communications, IEEE Transactions on*, vol. 44, no. 3, pp. 399–406, March 1996.

[7] M. Morelli, A. D'Andrea, and U. Mengali, "Feedforward ML-Based Timing Estimation with PSK Signals," *Communications Letters, IEEE*, vol. 1, no. 3, pp. 80–82, May 1997.

[8] Y. Wang, E. Serpedin, and P. Ciblat, "Blind Feedforward Cyclostationarity-Based Timing Estimation for Linear Modulations," *Wireless Communications, IEEE Transactions on*, vol. 3, no. 3, pp. 709–715, May 2004.

[9] W. Gappmair, S. Cioni, G. E. Corazza, and O. Koudelka, "Extended Gardner Detector for Improved Symbol-Timing Recovery of M-PSK Signals," *IEEE transactions on communications*, vol. 54, no. 11, pp. 1923–1927, Nov. 2006.

[10] F. M. Gardner, "Demodulator Reference Recovery Techniques Suited for Digital Implementation," ESA Final Report, ESTEC Contract No 6847/86/NL/DG, Tech. Rep., Aug. 1988.

[11] M. Moeneclaey and G. Ascheid, "Extension of the Viterbi and Viterbi Carrier Synchronization Algorithm to OQPSK Transmission," in *Proc. 2nd International Workshop on DSP Applied to Space Communications, Politecnico di Torino*, 1990, pp. 24–25.

[12] A. A. D'Amico, A. N. D'Andrea, and U. Mengali, "Feedforward Joint Phase and Timing Estimation with OQPSK Modulation," *Vehicular Technology, IEEE Transactions on*, vol. 48, no. 3, pp. 824–832, 1999.

[13] J. A. López-Salcedo and G. Vázquez, "Cyclostationary Joint Phase and Timing Estimation for Staggered Modulations," in *Acoustics, Speech, and Signal Processing, 2004. Proceedings.(ICASSP'04). IEEE International Conference on*, vol. 4. IEEE, 2004, pp. iv–833.

[14] U. Mengali and A. N. D'Andrea, *Synchronization Techniques for Digital Receivers*. Plenum Press, 1997.

[15] J. Mackenthun, K., "A Fast Algorithm for Multiple-Symbol Differential Detection of MPSK," *Communications, IEEE Transactions on*, vol. 42, no. 234, pp. 1471–1474, Feb 1994.

[16] H. L. Van Trees, *Detection, Estimation and Modulation, part I*. New York: Wiley, 1968.

[17] M. Meyers and L. Franks, "Joint Carrier Phase and Symbol Timing Recovery for PAM Systems," *Communications, IEEE Transactions on*, vol. 28, no. 8, pp. 1121–1129, Aug. 1980.

[18] W. Sweldens, "Fast Block Noncoherent Decoding," *IEEE communications letters*, vol. 5, no. 4, pp. 132–134, April 2001.

[19] R. H. Walden, "Analog-to-Digital Converter Survey and Analysis," *Selected Areas in Communications, IEEE Journal on*, vol. 17, no. 4, pp. 539–550, April 1999.

[20] A. N. D'Andrea, U. Mengali, and R. Reggiannini, "The Modified Cramér-Rao Bound and its Application to Synchronization Problems," *Communications, IEEE Transactions on*, vol. 42, no. 234, pp. 1391–1399, Feb./Mar./Apr. 1994.

[21] M. Moeneclaey, "A Comparison of Two Types of Symbol Synchronizers for which Self-Noise is Absent," *Communications, IEEE Transactions on*, vol. 31, no. 3, pp. 329–334, March 1983.

[22] C. Shaw and M. Rice, "The Cramér-Rao Bound for Joint Parameter Estimation of Burst-Mode QPSK," in *Military Communications Conference, 2009. MILCOM 2009. IEEE*, Oct 2009, pp. 1–7.

[23] M. Morelli and A. A. D'Amico, "Maximum likelihood timing and carrier synchronization in burst-mode satellite transmissions," *EURASIP Journal on Wireless Communications and Networking*, vol. 2007, 2007.

[24] M. K. Simon and D. Divsalar, "On the Optimality of Classical Coherent Receivers of Differentially Encoded M-PSK," *Communications Letters, IEEE*, vol. 1, no. 3, pp. 67–70, May 1997.

[25] G. Colavolpe, "Classical Coherent Receivers for Differentially Encoded M-PSK are Optimal," *IEEE Communications Letters*, vol. 8, no. 4, pp. 211–213, April 2004.